

1 **High efficiency ethanol-diesel dual-fuel combustion: A comparison** 2 **against conventional diesel combustion from low to full engine load**

3
4 Vinícius B. Pedrozo*, Ian May, Wei Guan, Hua Zhao

5 Centre for Advanced Powertrain and Fuels Research (CAPF), Brunel University London, Kingston
6 Lane, Uxbridge, Middlesex, UB8 3PH, United Kingdom

7 * Corresponding author. E-mail address: vinicius.pedrozo@brunel.ac.uk (V. B. Pedrozo).

8 9 **Keywords**

10 Ethanol; low carbon fuel; dual-fuel combustion; diesel engine; greenhouse gas emissions, tank-to-
11 wheels.

12 13 **Highlights**

- 14 - High efficiency dual-fuel combustion was demonstrated between 0.3 and 2.4 MPa IMEP.
- 15 - Up to 4.4% higher net indicated efficiency than conventional diesel combustion.
- 16 - Up to 90% lower nitrogen oxides emissions using identical engine testing conditions.
- 17 - The use of ethanol as a substitute for diesel can reduce greenhouse gas emissions.

18

Abstract

Comparisons between dual-fuel combustion and conventional diesel combustion (CDC) are often performed using different engine hardware setups, exhaust gas recirculation rates, as well as intake and exhaust manifold pressures. These modifications are usually made in order to curb in-cylinder pressure rise rates and meet exhaust emissions targets during the dual-fuel operation. To ensure a fair comparison, an experimental investigation into dual-fuel combustion has been carried out from low to full engine load with the same engine hardware and identical operating conditions to those of the CDC baseline. The experiments were executed on a single cylinder heavy-duty diesel engine at a constant speed of 1200 rpm and various steady-state loads between 0.3 and 2.4 MPa net indicated mean effective pressure (IMEP). Ethanol was port fuel injected while diesel was direct injected using a high pressure common rail injection system. The start of diesel injection was optimised for the maximum net indicated efficiency in both combustion modes. Varied ethanol energy fractions and adaptive diesel injections were required to control the in-cylinder pressure rise rate and achieve highly efficient and clean dual-fuel operation. In terms of performance, the dual-fuel combustion attained higher net indicated efficiency than the CDC mode from 0.6 to 2.4 MPa IMEP, with a maximum of 47.2% at 1.2 MPa IMEP. The comparison also shows the use of ethanol resulted in 26% to 90% lower nitrogen oxides (NO_x) emissions than the CDC operation. At the lowest engine load of 0.3 MPa IMEP, the dual-fuel operation led to simultaneous low NO_x and soot emissions at the expense of a relatively low net indicated efficiency of 38.9%. In particular, the reduction in NO_x emissions introduced by the utilisation of ethanol has the potential to decrease the engine running costs via lower consumption of aqueous urea solution in the selective catalyst reduction system. Moreover, the dual-fuel combustion with a low carbon fuel such as ethanol is an effective means of decreasing the use of fossil fuel and associated greenhouse gas emissions.

1. Introduction

Heavy-duty (HD) vehicles are typically powered by diesel engines due to their cost-effectiveness and high fuel conversion efficiency. However, there is a lot of concern over the greenhouse gas (GHG) emissions produced from the combustion of diesel and other fossil fuels [1]. This is due to a recent increase in the atmospheric concentration of GHGs such as carbon dioxide (CO₂) [2], which can lead to irreversible changes in climate and cause impacts on natural and human systems on all continents and across the oceans [1].

In 2010, HD vehicles were responsible for approximately 34% of the GHGs emitted by the global transport sector and 46.5% of the road transport CO₂ emissions [3]. The disproportionate contribution is highlighted by the fact the HD fleet represents only 11% of the world motor vehicles [4]. Substantial and sustained reductions in fossil fuel energy use and GHG emissions have to be attained in order to address the transport sector's impact on the environment.

Additionally, conventional diesel combustion (CDC) incurs a wide range of local in-cylinder gas temperatures and fuel/air equivalence ratios that can lead to the formation of noxious emissions, such as NO_x and soot [5,6]. NO_x emissions are mainly formed in near-stoichiometric high temperatures regions close to the diesel diffusion flame [7]. Soot formation occurs in high fuel/air equivalence ratio and intermediate temperature zones within the diesel spray [8,9]. These pollutants are linked to premature deaths caused by cardiovascular and respiratory diseases [10,11].

Stringent fuel conversion efficiency and exhaust emissions regulations have been implemented to limit the levels of GHG and noxious emissions from HD vehicles [12][13][14][15]. Manufactures are incorporating costly engine design elements [16–20] and aftertreatment technologies [21,22] to comply with these emissions standards while achieving the GHG reduction targets [12][13]. Some

71 examples are the use of more robust selective catalyst reduction (SCR) systems for NOx
72 mitigation, flexible and high pressure diesel injection equipment, as well as high efficiency
73 turbocharging and air handling systems.

74
75 A balance between engine running costs and exhaust emissions can represent a challenge for HD
76 engine manufactures with the use of both advanced in-cylinder and aftertreatment measures
77 [16][17]. An improvement of 1% in fuel conversion efficiency can increase the levels of engine-out
78 NOx from 10 g/kWh to 14 g/kWh [18]. This adversely affects the total cost of ownership due to a
79 higher consumption of aqueous urea solution in the SCR system [23–26]. On the other hand, CDC
80 operation with very low engine-out NOx emissions can result in low fuel conversion efficiency and
81 excessive levels of soot due the different formation mechanisms [27,28].

82
83 Previous studies into dual-fuel compression ignition combustion have demonstrated the strategy
84 has the potential to tackle these issues, increasing the fuel conversion efficiency while decreasing
85 both the NOx and soot emissions [6][29][30][31][32]. This has been attributed to simultaneous
86 reductions in local fuel/air equivalence ratios, combustion temperatures, and heat transfer losses
87 [6][32].

88
89 Figure 1 shows an example of a dual-fuel system, which can be achieved by the installation of a
90 port fuel injection system of a low reactivity fuel such as gasoline [32], ethanol [33], or natural gas
91 [34] on a diesel engine. The ignition of the premixed charge is generally triggered by direct
92 injections of diesel [6][35]. It should be noted that the use of a low carbon fuel like ethanol
93 [36][37][38][39] can help decrease the dependence on fossil fuels and minimise GHG emissions
94 from the global transport sector [40].

95
96 Despite the advantages of the dual-fuel operation, it is often challenging to obtain direct
97 comparisons against the CDC mode from low to high engine loads (e.g. above 2.0 MPa IMEP).

This is due to modifications in engine hardware and/or test conditions that help control the emissions of NO_x and the in-cylinder pressure rise rates from dual-fuel combustion. These alterations typically include the use of a different piston design and/or compression ratio [41][42] as well as changes in the levels of exhaust gas recirculation [43].

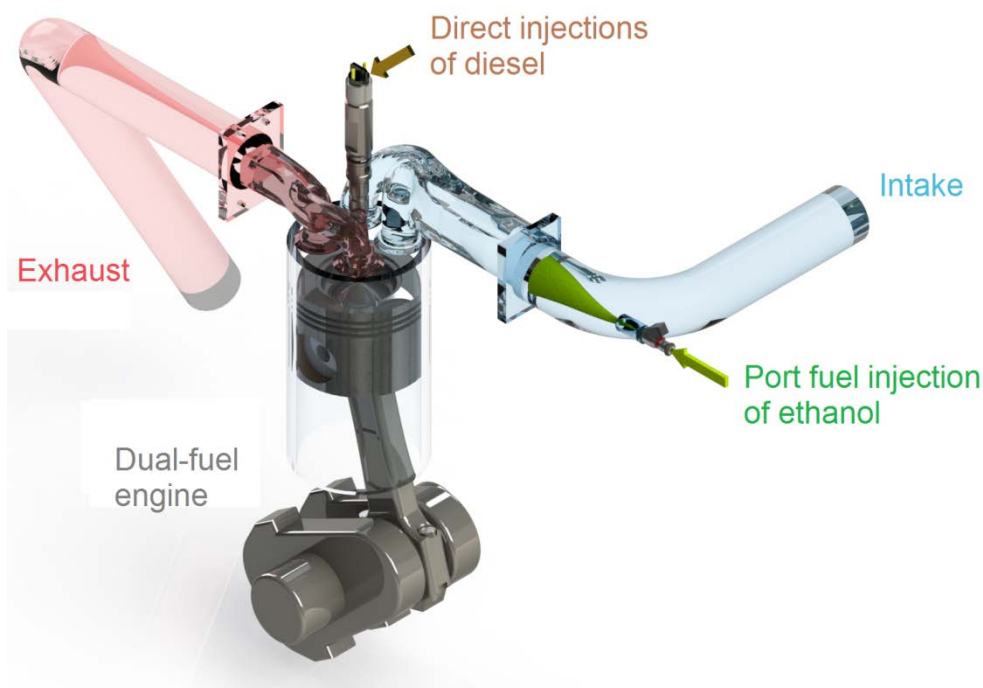


Figure 1 – Schematic diagram of a dual-fuel engine with direct injections of diesel and port fuel injection of ethanol.

This study aims at exploring the potential of dual-fuel combustion to achieve high fuel conversion efficiency and low exhaust emissions using the same combustion system and identical engine testing conditions to those employed by the CDC baseline.

To the best of our knowledge, this is the first attempt to experimentally compare the controllability, emissions, and fuel conversion efficiency of ethanol-diesel dual-fuel operation to those of the CDC mode from low (0.3 MPa IMEP) to full engine load (2.4 MPa IMEP). Moreover, practical considerations have been raised and the potential CO₂ reduction has been discussed on both a tank-to-wheels and well-to-wheels basis [37][44].

The investigation was performed on a single cylinder HD diesel engine at a steady-state speed of 1200 rpm. The diesel injection timings and the number of injections per cycle were optimised in both the combustion modes in order to maximise the fuel conversion efficiency, which was given by the net indicated efficiency. In addition, the dual-fuel operation was carried out using ethanol energy fractions that achieved the highest net indicated efficiency with minimal NO_x and soot emissions, as determined in our previous studies [29][30][31][45][46].

2. Experimental setup

2.1. Experimental facilities

A schematic diagram of the single cylinder HD engine experimental setup is shown in Figure 2. A Froude Hofmann AG150 eddy current dynamometer was used to absorb the power produced by the engine. Fresh intake air was supplied to the engine via an AVL 515 sliding vanes compressor with a closed loop control for the boost pressure. A throttle valve located upstream of a large-volume surge tank provided fine control over the intake manifold pressure. The fresh air mass flow rate (\dot{m}_{air}) was measured with an Endress+Hauser Proline t-mass 65F thermal mass flow meter.

Another surge tank was installed in the exhaust manifold to damp out pressure fluctuations prior to the exhaust gas recirculation (EGR) circuit. An electronically controlled butterfly valve located downstream of the exhaust surge tank was used to set the required back pressure (e.g. exhaust manifold pressure). High-pressure loop cooled external EGR was supplied to the engine intake system by opening a pulse width modulation-controlled EGR valve. Boosted intake air and external EGR temperatures were controlled using water cooled heat exchangers.

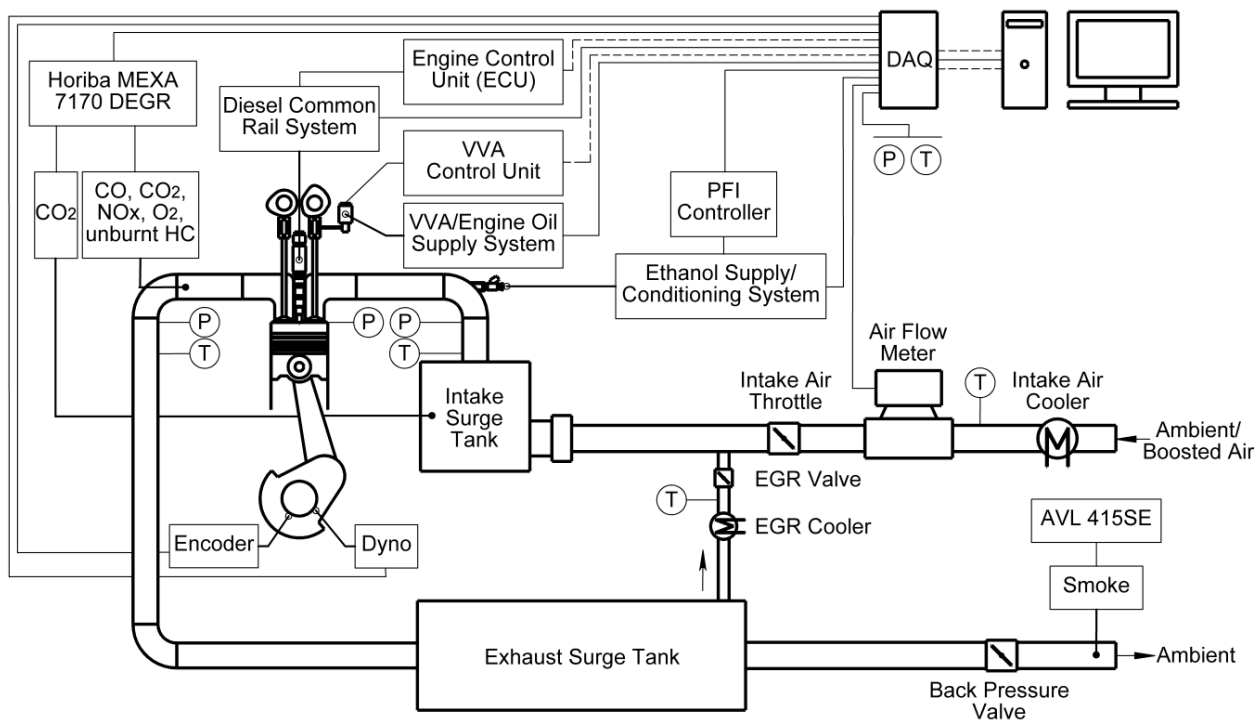


Figure 2 – Schematic diagram of the engine experimental setup.

2.2. Engine specifications

The single cylinder HD engine was equipped with port fuel injection of ethanol and high pressure common rail direct injection of diesel. The combustion system consisted of a 4-valve cylinder head and a stepped-lip piston bowl design with a geometric compression ratio of 16.8. Base hardware specifications are outlined in Table 1.

The diesel injections were controlled via a dedicated engine control unit (ECU) with the ability to support up to three shots per cycle. The intake valve lift profile was adjusted via a lost-motion variable valve actuation (VVA) system based on a normally open high-speed solenoid valve assembly and a special intake cam design [47].

Coolant and oil pumps were not coupled to the engine and were driven by separate electric motors. Engine coolant and oil temperatures were set to 353 ± 3 K. The oil pressure was held at 450 ± 10 kPa throughout the experiments.

160

161 Table 1 – Single cylinder HD engine specifications.

Parameter	Value
Displaced volume	2.026 dm ³
Stroke	155 mm
Bore	129 mm
Connecting rod length	256 mm
Number of valves	4
Piston type	Stepped-lip bowl
Geometric compression ratio	16.8
Peak in-cylinder pressure (P_{\max}) limitation	18 MPa
Diesel Injection System	Bosch common rail, injection pressure of 50–220 MPa, 8 holes with nominal diameter of 0.176 mm, included spray angle of 150°
Ethanol Injection System	PFI Marelli IWP069, included spray angle of 15°

162

163 2.3. Fuel properties and delivery

164

165 The relevant properties of the fuel used in this work are listed in Table 2. The diesel fuel was
 166 supplied to the engine using a high pressure common rail injection system. Two Endress+Hauser
 167 Promass 83A Coriolis flow meters were used to determine the diesel mass flow rate (\dot{m}_{diesel}) by
 168 measuring the total fuel supplied to and from the diesel high pressure pump and injector.

169

170 In order to allow for dual-fuel operation, an ethanol fuel injection system was designed and fitted to
 171 the engine. Ethanol was injected through a port fuel injector (PFI) installed in the intake manifold.
 172 An in-house injector driver controlled the injector pulse width, which was adjusted according to the
 173 desired ethanol energy fraction.

174

175 The ethanol mass flow rate ($\dot{m}_{ethanol}$) was measured using an Endress+Hauser Proline Promass
 176 80A Coriolis flow meter, allowing for measurements with an accuracy of 0.15%. The injection
 177 pressure was continuously monitored by a pressure transducer, so that a constant relative
 178 pressure of 300 kPa could be maintained across the injector.

179

180 Table 2 – Fuel properties.

Property	Diesel	Ethanol
Product name	Red diesel (gas oil)	Absolute ethanol 100
Standard/specification	BS 2869 Class A2	Anhydrous ethanol
Density at 293 K (ρ_{fuel})	0.827 kg/dm ³	0.790 kg/dm ³ [48]
Cetane number	> 45	n/a
Research octane number (RON)	n/a [49]	~107 [49]
Alcohol content in volume	n/a	99.9%
Water content	< 0.20 g/kg [50]	1.7 g/kg [48]
Sulphur content	< 0.01 g/kg	n/a
Heat of vaporisation	270 kJ/kg [49]	840 kJ/kg [49]
Carbon mass content ($\%C_{fuel}$)	86.6%	52.1% [49]
Hydrogen mass content ($\%H_{fuel}$)	13.2%	13.1% [49]
Oxygen mass content ($\%O_{fuel}$)	0.2%	34.8% [49]
Normalised molecular composition	$CH_{1.825}O_{0.0014}$	$CH_3O_{0.5}$
Lower heating value (LHV_{fuel})	42.9 MJ/kg	26.9 MJ/kg [49]

181

182 2.4. Exhaust emissions measurements and analysis

183

184 An AVL 415SE smoke meter was used for soot emissions measurements downstream of the back
185 pressure valve. Gaseous emissions such as NO_x, CO₂, carbon monoxide (CO), oxygen (O₂), and
186 unburnt hydrocarbon (HC) were taken with a Horiba MEXA-7170 DEGR emissions analyser. The
187 EGR rate was determined by calculating the ratio of the intake to the exhaust manifold CO₂
188 concentration measured by the same emissions analyser. A high pressure module allowed for
189 high-pressure sampling upstream of the back pressure valve while a heated line was used to
190 prevent condensation.

191

192 The measurement of unburnt HCs was performed on a wet basis by the Horiba's heated flame
193 ionisation detector (FID). However, the HC emissions measured with the FID can lead to
194 misinterpretation of the results due to the relative insensitivity of the device towards alcohols and
195 aldehydes [51,52]. Therefore, the FID response was corrected by the method developed by Kar
196 and Cheng [51] with an updated response factor of 0.68 for the oxygenated organic species

197 resultant from ethanol combustion [52]. This procedure has been reported in our previous work
198 [31] and allows for the determination of the actual unburnt HC emissions.

199
200 Finally, the exhaust emissions measurements were converted to net indicated specific emissions
201 using the methodology described in the Regulation number 49 of the Economic Commission for
202 Europe of the United Nations [50]. The concentrations of CO and NO_x were converted to a wet
203 basis by applying a correction factor for the raw exhaust gas according to the in-cylinder fuel
204 mixture composition.

205 206 2.5. Data acquisition

207
208 The in-cylinder pressure was measured by a Kistler piezoelectric pressure sensor Type 6125C.
209 Under mechanical load, crystals in the sensor produced an electrostatic charge, which was
210 converted into an electric potential difference by means of an AVL FI Piezo charge amplifier.
211 Intake and exhaust manifold pressures were measured by two Kistler water cooled piezoresistive
212 absolute pressure sensors Type 4049A coupled to Kistler amplifiers Type 4622A. Temperatures
213 and pressures at relevant locations were measured by K-type thermocouples and pressure
214 gauges, respectively.

215
216 Two National Instruments data acquisition (DAQ) cards and a personal computer were used to
217 acquire the signals from the measurement device. An USB-6251 high speed DAQ card received
218 the crank angle resolved data synchronized with an optical encoder of 0.25 crank angle degrees
219 (CAD) resolution. An USB-6210 low speed DAQ card acquired the low frequency engine operation
220 conditions. These data were displayed live by an in-house developed DAQ program and
221 combustion analyser.

222

2.6. Data analysis

A relevant parameter for the dual-fuel operation was the ethanol energy fraction (EF), which was defined as the ratio of the energy content of the ethanol to the total fuel energy supplied by

$$EF = \frac{\dot{m}_{ethanol} LHV_{ethanol}}{(\dot{m}_{ethanol} LHV_{ethanol}) + (\dot{m}_{diesel} LHV_{diesel})} \quad (1)$$

The excess of fuel in the exhaust gas was given by the global fuel/air equivalence ratio (Φ), which was calculated as

$$\phi = \frac{(14.5 \dot{m}_{diesel} + 9.0 \dot{m}_{ethanol})}{\dot{m}_{air}} \quad (2)$$

Crank angle based in-cylinder pressure traces were averaged over 200 consecutive cycles for each operating point and used to calculate the IMEP and the apparent net heat release rate (HRR). The pressure rise rate (PRR) was represented by the average of the maximum pressure variations of 200 cycles of cylinder pressure versus crank angle. Combustion and in-cylinder flow stability were monitored by the coefficient of variation of IMEP (COV_{IMEP}) and P_{max} (COV_{P_{max}}) over the sampled cycles.

Since the absolute value of the heat released is not as important to this study as the bulk shape of the curve with respect to crank angle, a constant ratio of specific heats (γ) of 1.33 was assumed throughout the engine cycle. The mass fraction burnt (MFB) was given by the ratio of the integral of the HRR and the maximum cumulative heat release. Combustion phasing was determined by the crank angle of 50% (CA50) cumulative heat release. Combustion duration was represented by

249 the period of time between the crank angles of 10% (CA10) and 90% (CA90) cumulative heat
250 release.

251
252 A current probe was used to acquire the electric current signal sent from the ECU to the diesel
253 injector solenoid. The signal was corrected by adding the respective energising time delay, which
254 was previously measured in a constant volume chamber [53]. The resulting diesel injector current
255 signal allowed for the determination of the actual start of diesel injection.

256
257 Ignition delay was defined as the period of time between the actual start of main diesel injection
258 (SOI_main) and the start of combustion (SOC), set to 0.3% MFB point of the averaged cycle. After
259 the calculation of the combustion characteristics (e.g. CA50) and ignition delay, the average in-
260 cylinder pressure and the resulting HRR were smoothed using a Savitzky-Golay filter.

261
262 Net indicated efficiency was determined by calculating the ratio of the work done to the rate of fuel
263 energy supplied to the engine. Combustion efficiency calculations were based on the emissions
264 products not fully oxidised during the combustion process except soot.

266 3. Methodology

267
268 Figure 3 shows the location of the test points over an estimated speed and load map of a HD
269 diesel engine. Testing was carried out under a steady-state engine speed of 1200 rpm over a
270 range of loads from 0.3 to 2.4 MPa IMEP. A PRR of 2.0 MPa/CAD and a P_{max} of 18 MPa were
271 considered as the upper bounds for calibration. Stable engine operation was quantified by
272 COV_IMEP values less than 5%.

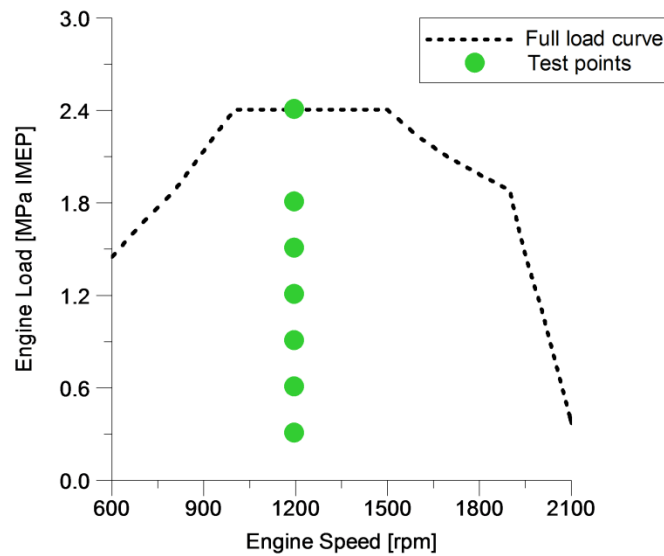


Figure 3 – Experimental test points over an estimated HD diesel engine speed-load map.

Table 3 summarises the test conditions for the CDC and ethanol-diesel dual-fuel operating modes. The experiments were performed using a pressure-based effective compression ratio of 16.8 [46]. The expansion ratio remained constant as a result of the fixed exhaust camshaft timing.

Table 3 – Operating conditions for the CDC and ethanol-diesel dual-fuel operation from low to full engine load at 1200 rpm.

Engine load MPa IMEP	Intake manifold pressure	Exhaust manifold pressure	Intake manifold air temp.	EGR rate %	Diesel injection pressure	
	kPa	kPa	K		(CDC) MPa	(Dual-fuel) MPa
0.3	115	125	307	25	105	50
0.6	125	135	310	25	125	90
0.9	155	165	315	25	140	110
1.2	190	200	319	25	155	125
1.5	230	240	324	25	170	140
1.8	260	270	324	20	190	160
2.4	300	310	323	11	220	190

The intake manifold pressure set point was taken from a Euro V compliant multi-cylinder HD diesel engine in order to provide a sensible starting point, since an external boosting device was used in place of a turbocharger. The exhaust manifold pressure was varied to maintain a constant

287 pressure differential across the cylinder of 10 kPa. This allowed for exhaust gas recirculation,
288 which was used to curb NO_x formation.

289
290 The EGR rate was limited at 25% between 0.3 and 1.5 MPa IMEP to avoid excessive smoke and
291 a decrease in net indicated efficiency. At 1.8 and 2.4 MPa IMEP, the EGR rate was reduced to
292 20% and 11%, respectively. This was essential in order to achieve lean and efficient high load
293 operations using the same levels of boost pressure of the multi-cylinder engine.

294
295 Diesel injection pressures were set to be 30 to 55 MPa higher in the CDC mode than those in the
296 dual-fuel combustion due to the relatively higher diesel flow rates and longer injection durations at
297 a given engine load. This was necessary to minimise soot emissions from the CDC operation via
298 improved diesel atomisation and enhanced the fuel-air mixing process.

299
300 All comparisons were carried out for the cases that attained the highest net indicated efficiencies
301 after sweeps of diesel injection timings. Additionally, the diesel injection strategy (i.e. number of
302 diesel injections per cycle) was optimised and varied as the engine load was increased.

303
304 In the dual-fuel mode, the ethanol energy fraction was also optimised for minimum NO_x and soot
305 emissions, as supported by our previous dual-fuel studies [29][30][31][45][46]. A maximum EF of
306 0.79 was achieved at 1.2 MPa IMEP. Advanced dual-fuel combustion control strategies such as
307 the internal exhaust gas recirculation (iEGR) [31] and Miller cycle [46] were not explored in this
308 study as they would require different test procedures.

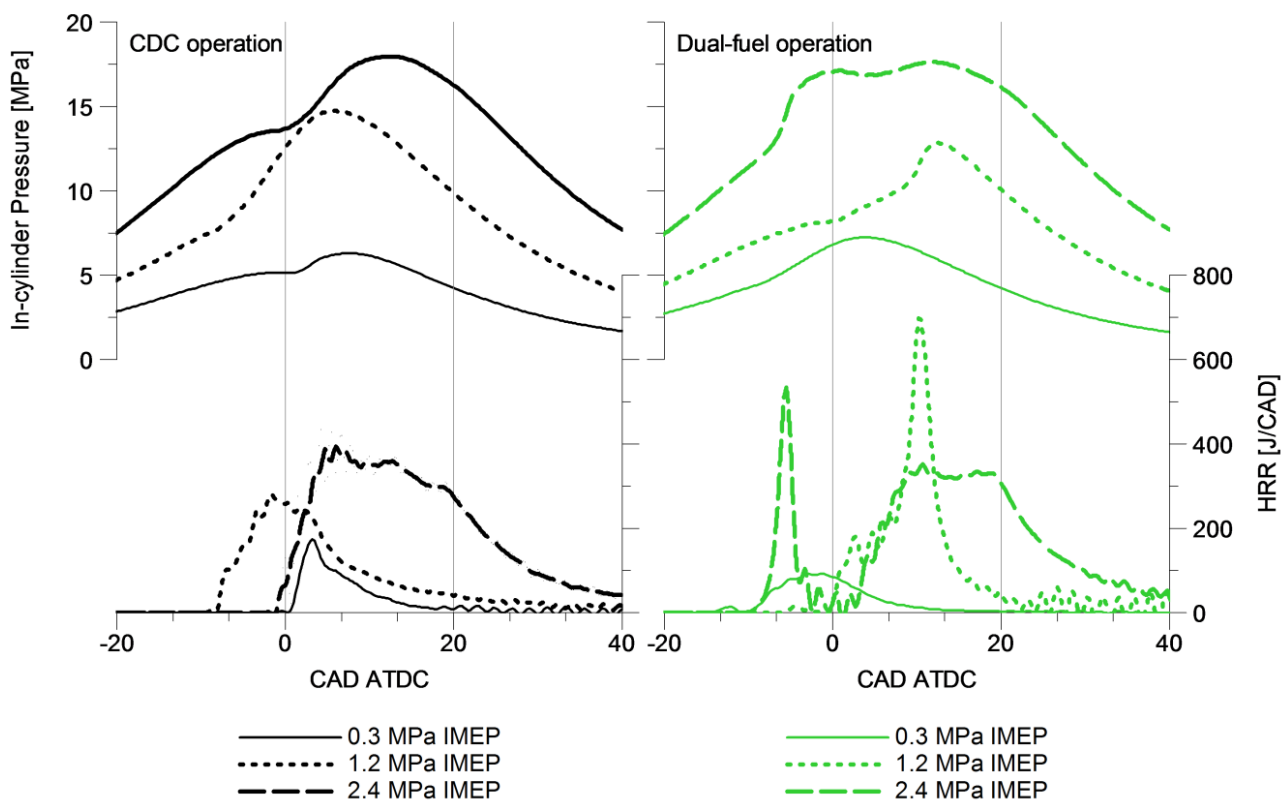
309 310 **4. Results and Discussion**

311 312 4.1. Overview of the load sweep

313

314 Figure 4 depicts the effect of engine load on both the operating modes. CDC operation was
 315 characterised by longer mixing-controlled combustion phase as the load was increased. This was
 316 attributed to longer diesel injection periods and increased amount of fuel, which limited the fuel
 317 vapour-air mixing process [49,54]. The optimum CA50 in CDC mode varied as the engine load
 318 was increased, allowing for more advanced burn rates at mid-loads and delayed combustion
 319 events at high loads. The reasons behind this are described in the next subsection.

320



321

322 Figure 4 – The effect of engine load on CDC and ethanol-diesel dual-fuel operation at 1200 rpm.

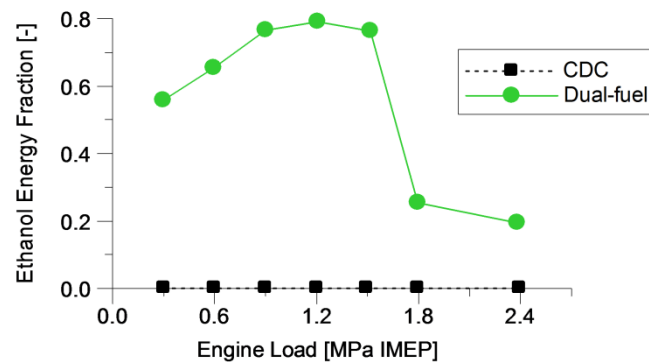
323

324 The dual-fuel operation led to higher peak heat release than the CDC mode at all engine loads
 325 except 0.3 MPa IMEP. This required different diesel injection strategies and eventually later
 326 combustion process in order to control the PRRs as the engine load was increased. The
 327 combustion was triggered by and initiated after the diesel injection at low and medium load
 328 operations between 0.3 and 1.5 MPa IMEP. Higher compression pressures and temperatures
 329 accelerated the autoignition of the premixed ethanol fuel prior to the diesel injection at high engine
 330 loads of 1.8 and 2.4 MPa IMEP.

331

332 Figure 5 shows the optimum EF had to be rapidly reduced from 0.76 to 0.25 when increasing the
 333 engine load from 1.5 to 1.8 MPa IMEP. This was necessary in order to minimise the PRRs
 334 associated with the early autoignition of ethanol. It is important to bear in mind that modifications in
 335 the engine hardware (e.g. lower effective compression ratio via Miller cycle) and/or test procedure
 336 (e.g. lower intake manifold air temperature) can increase the maximum EF at higher loads [46].

337



338

339 Figure 5 – Optimum ethanol energy fraction for varied engine loads at 1200 rpm.

340

341 4.2. Combustion control

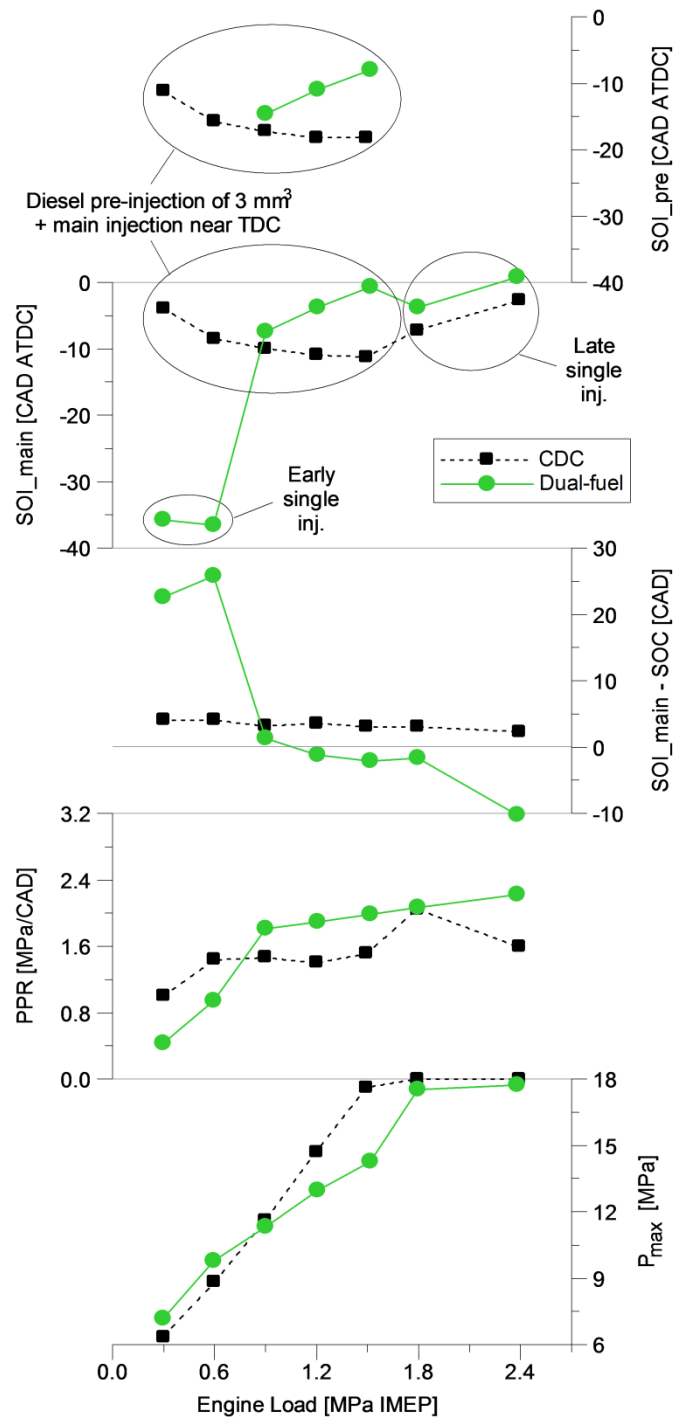
342

343 Figure 6 shows the actual start of diesel pre-injection (SOI_{pre}), SOI_{main}, and in-cylinder
 344 pressure characteristics for optimised CDC and dual-fuel operation. In the CDC mode, a 3 mm³
 345 diesel pre-injection with a constant dwell time of 1 ms was used to reduce the levels of PRR [45]
 346 between the engine loads of 0.3 MPa IMEP and 1.5 MPa IMEP. The lower PRRs were associated
 347 with the shorter ignition delay produced by the combustion of the diesel pre-injection and likely
 348 formation of a hot and reactive mixture prior to the main diesel injection [55].

349

350 At high engine loads of 1.8 and 2.4 MPa IMEP, relatively shorter ignition delays introduced by
 351 lower EGR rates and higher in-cylinder pressures and temperatures allowed for the use of a single
 352 diesel injection near firing top dead centre (TDC). The maximum SOI_{main} advance was limited
 353 by the P_{max} while the PRRs were maintained within the limit of 2.0 MPa/CAD.

354



355

356

Figure 6 – Diesel injection timings and combustion characteristics for optimised CDC and ethanol-diesel dual-fuel operation at 1200 rpm.

357

358

359

In the dual-fuel operation, the combination of an early single diesel injection at about -36 CAD after top dead centre (ATDC) and EFs of 0.56 and 0.65 allowed for long ignition delays (SOI_main–SOC) and better mixture preparation at 0.3 and 0.6 MPa IMEP. This enhanced the

361

362 combustion process via a more progressive and probably sequential combustion from high to low
363 reactivity regions [8]. This has also been identified in computational simulations performed by
364 Desantes et al. [56] and is supported by the low levels of PRR. However, the P_{max} was increased
365 when compared to that of the CDC operation due to earlier CA50 and shorter combustion for the
366 dual-fuel mode at these particular loads (see Figure 7).

367
368 At mid-loads between 0.9 and 1.5 MPa IMEP, less partially premixed diesel fuel could be used in
369 order to prevent an early ignition of the in-cylinder charge. Therefore, the mass of the diesel was
370 divided into two direct injections using the same strategy employed in the CDC cases. The
371 injection of a small amount of diesel prior to the SOI_main was essential to mitigate excessive
372 PRRs. This was a result of a shorter SOI_main–SOC period and elimination of the premixed
373 combustion peak typically observed with a late single diesel injection strategy [45]. Despite the
374 controlled levels of PRR, the diesel injection timings were delayed by up to 10.5 CAD when
375 compared against those of the CDC operation, helping lower the P_{max} levels.

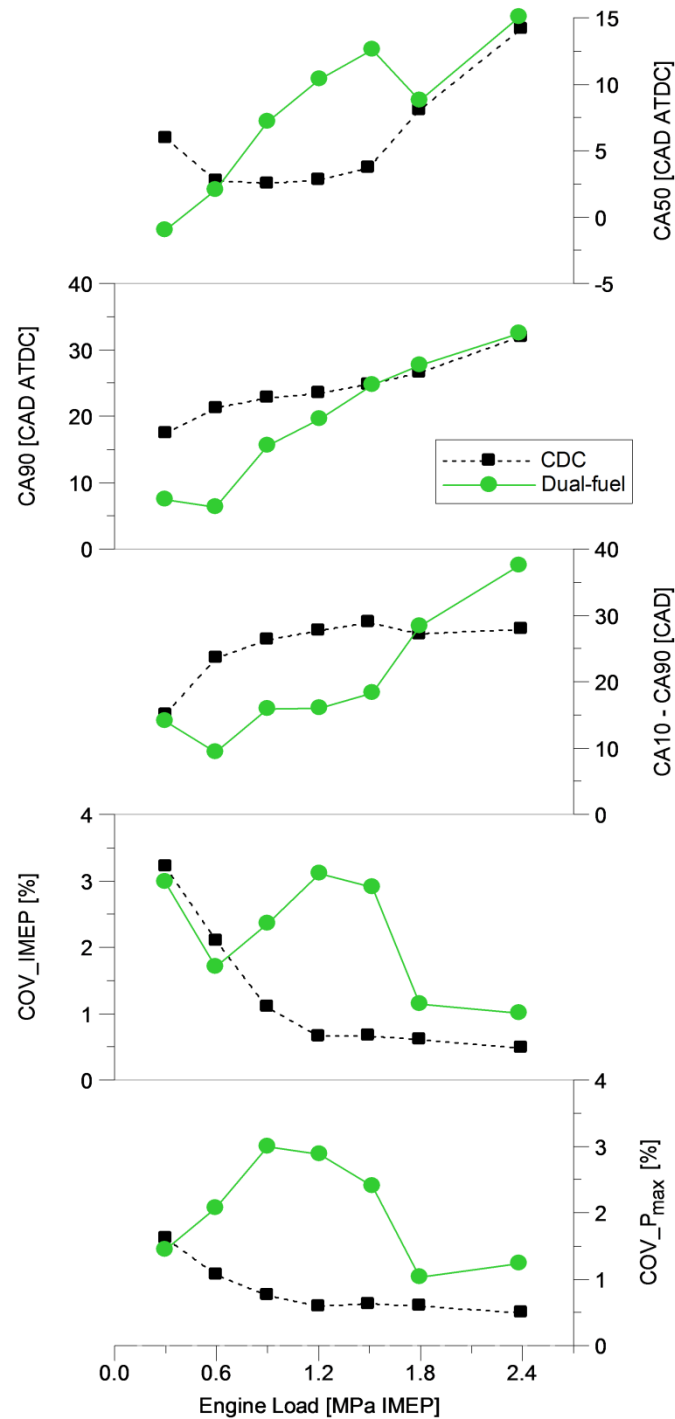
376
377 At 1.8 and 2.4 MPa IMEP, the premixed ethanol fuel autoignited prior to the diesel injection. Lowe
378 ethanol energy fractions and a single diesel injection near TDC were used to control the burn rate
379 as well as the resulting PRR and P_{max} . The introduction of a diesel pre-injection would increase the
380 PRR levels at these loads due to simultaneous and early combustion of the ethanol and pre-
381 injected diesel fuel.

382 383 4.3. Heat release analysis

384
385 Figure 7 depicts the heat release characteristics for the CDC and dual-fuel operation. The
386 optimum CA50 for the maximum net indicated efficiency was initially advanced and then retarded
387 in the CDC mode. The advance in the CA50 position was likely linked to the short CA10–CA90
388 period and relatively higher heat transfer losses at 0.3 MPa IMEP. The delay was associated with

389 the peak in-cylinder pressure limitation at high load operations of 1.8 and 2.4 MPa IMEP.
 390 Additionally, lower levels of EGR and possibly higher combustion temperatures helped shorten the
 391 CA10–CA90 periods of the CDC operation at these high load conditions.

392



393

394 Figure 7 – Heat release characteristics for optimised CDC and ethanol-diesel dual-fuel operation

395

at 1200 rpm.

396

In comparison, the dual-fuel operation often required later CA50s as the engine load was increased in order to avoid excessive PRRs. At high loads of 1.8 and 2.4 MPa IMEP, the CA50 and CA90 positions were similar for both the combustion modes due to the P_{\max} limitation of 18 MPa and lower EFs used in the dual-fuel mode.

In general, the increase in engine load generally led to later CA90s and longer CA10–CA90 as a result of the higher fuel flow rates. The higher degree of premixed combustion in the dual-fuel mode was likely the cause for the relatively earlier CA90s and faster CA10–CA90 periods between 0.3 and 1.5 MPa IMEP. Nonetheless, the early ignition of the ethanol fuel produced longer burn rates than the CDC operation at 1.8 and 2.4 MPa IMEP.

In terms of combustion stability, the mixing-controlled combustion of the CDC operation effectively decreased the COV_{IMEP} and COV_{P_{max}} to 0.5% as the engine load was increased to 2.4 MPa IMEP. In the dual-fuel mode, later CA50s and a more premixed combustion yielded higher levels of COV_{IMEP} between 0.9 and 2.4 MPa IMEP. In addition, the dual-fuel operation resulted in higher COV_{P_{max}} at all engine loads except 0.3 MPa IMEP. Nevertheless, the COV_{IMEP} and COV_{P_{max}} could be controlled between 1.0% and 3.0%.

4.4. Engine-out emissions

Figure 8 shows the net indicated specific emissions for the optimum cases over a sweep of load. An EGR rate of 25% was used to minimise NO_x emissions at engine loads up to 1.5 MPa IMEP. This allowed for a CDC operation with net indicated specific emissions of NO_x (ISNO_x) of 3.9 g/kWh, on average, between 0.3 and 1.5 MPa IMEP. The use of lower EGR rates of 20% and 11% increased the combustion temperatures at 1.8 and 2.4 MPa IMEP, yielding higher ISNO_x of 4.4 and 5.7 g/kWh, respectively.

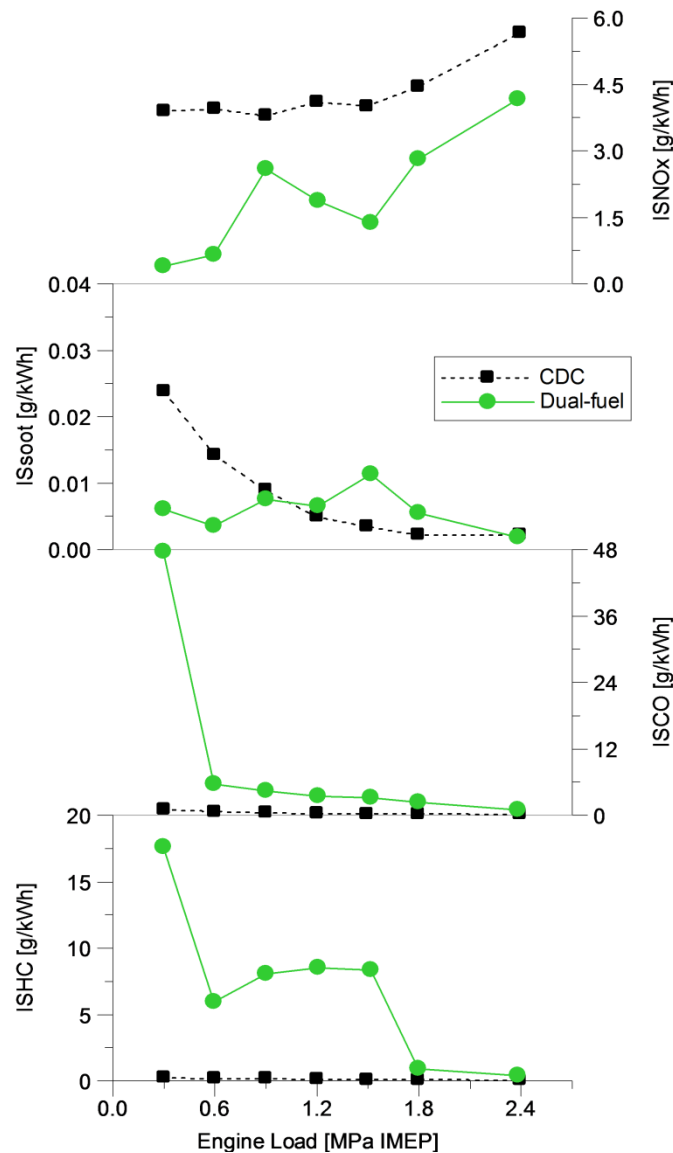


Figure 8 – Net indicated specific emissions for optimised CDC and ethanol-diesel dual-fuel operation at 1200 rpm.

Alternatively, the optimised dual-fuel operation achieved lower ISNO_x than the CDC mode at all engine loads. This was linked to the premixed ethanol fuel, which probably helped decrease the amount of in-cylinder regions of high combustion temperature. Reductions in NO_x emissions varied from 26% at 2.4 MPa IMEP up to 90% at 0.3 MPa IMEP for EFs of 0.19 and 0.56, respectively.

The lowest levels of ISNO_x were attained at 0.3 and 0.6 MPa IMEP due to longer ignition delays and relatively more homogenous combustion process when compared against the other dual-fuel

436 cases with diesel injections closer to TDC. NO_x emissions were decreased when increasing the
437 engine load from 0.9 to 1.5 MPa IMEP due to later optimum CA₅₀s and potentially lower
438 combustion temperatures. At high loads of 1.8 and 2.4 MPa IMEP, the ethanol autoignition
439 process and shorter diesel mixing-controlled combustion helped reduce the peak in-cylinder gas
440 temperatures [46], decreasing the ISNO_x when compared to the CDC operation.

441
442 In the CDC mode, higher diesel injection pressures and in-cylinder gas temperatures helped curb
443 soot emissions as the engine load was increased. In comparison, net indicated specific emissions
444 of soot (ISsoot) were maintained consistently low in the dual-fuel operation because of reduced
445 regions of fuel rich combustion, particularly at 0.3 and 0.6 MPa IMEP. This is a significant
446 improvement over the CDC cases considering the dual-fuel combustion employed lower diesel
447 injection pressures, as explained in Section 3.

448
449 At a mid-load of 1.5 MPa IMEP, the dual-fuel operation yielded an ISsoot of 0.011 g/kWh, which
450 was significantly higher than the 0.003 g/kWh for the CDC case. This can be explained by the late
451 CA₅₀ position and short ignition delay, which potentially reduced combustion temperatures and
452 increased local fuel/air equivalence ratios.

453
454 CO and unburnt HC emissions increased significantly in the dual-fuel combustion when compared
455 against the CDC operation. This was probably a result of premixed fuel trapped in the crevice
456 volumes of the stock diesel piston as well as lower local in-cylinder gas temperatures [6].

457
458 High net indicated specific emissions of CO (ISCO) and unburnt HC (ISHC) were measured for the
459 dual-fuel operation at 0.3 MPa IMEP. This can be attributed to excessively low combustion
460 temperatures and overly lean regions that did not release enough heat in order to effectively
461 oxidise the fuel [6]. At 1.8 and 2.4 MPa IMEP, the use of lower EFs as well as lower EGR rates
462 likely increased combustion temperatures, decreasing CO and unburnt HC emissions.

4.5. Engine performance

Figure 9 depicts the engine performance metrics for optimised CDC and ethanol-diesel dual-fuel operation. The global fuel/air equivalence ratio (Φ) of the dual-fuel combustion was either comparable or lower than that of the CDC mode at a given engine load. This was attributed to minor variations in the intake air flow rate (within 3% and not showed for the sake of brevity) and improvements in net indicated efficiency. Differences in LHV_{fuel} probably balanced out changes in stoichiometric air/fuel ratio.

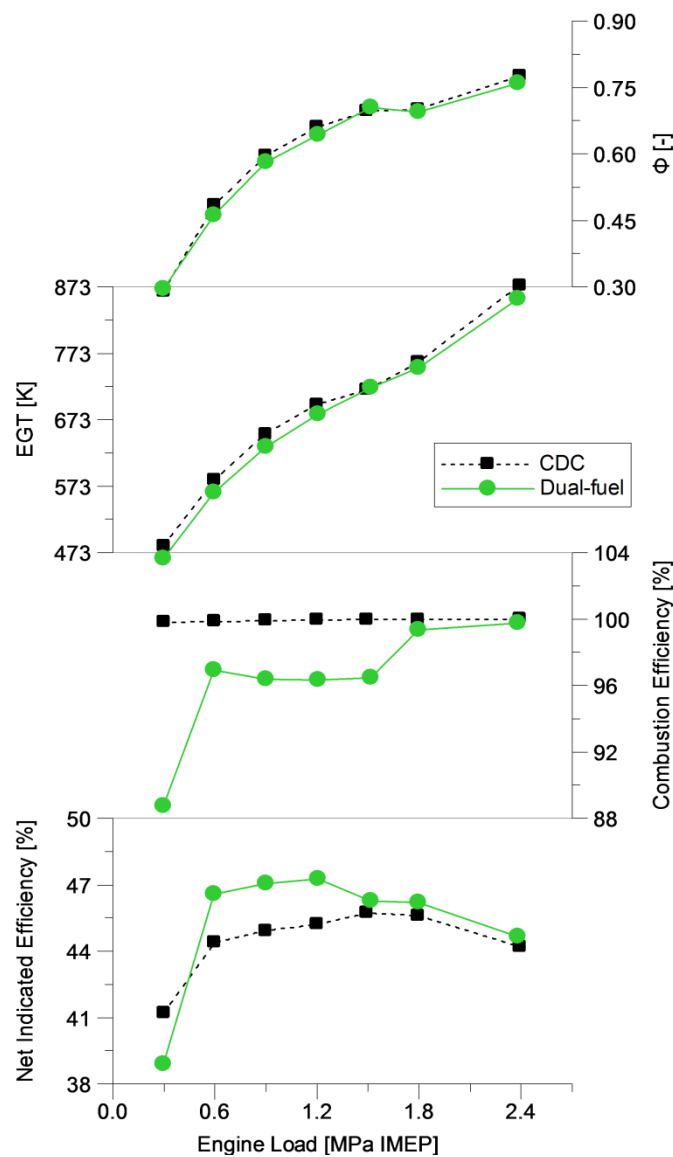


Figure 9 – Engine performance for optimised CDC and ethanol-diesel dual-fuel operation at 1200 rpm.

475 The exhaust gas temperature (EGT) increased with the engine load due to later CA90s and higher
476 levels of fuel energy supplied. However, the dual-fuel operation incurred EGTs up to 20 K lower
477 than those of the respective CDC case. This was possibly a result of a more homogenous and
478 lower temperature combustion process for an engine operation with premixed ethanol fuel [31][46].

479
480 The dual-fuel mode also yielded lower combustion efficiencies than the CDC cases as supported
481 by the ISCO and ISHC in Figure 8. At medium and high engine loads, combustion efficiency
482 ranged between 96.3% and 99.7% despite the use of high EFs. This was attributed to relatively
483 higher Φ and local in-cylinder gas temperatures.

484
485 At the lowest load of 0.3 MPa IMEP, the combination of a low combustion efficiency of 88.7% and
486 an EGT of 463 K can represent a challenge for HD engine manufactures. This is due to a
487 reduction in the effectiveness of the oxidation catalyst in reducing CO and unburnt HC emissions
488 [57][58]. In-cylinder control strategies such as intake throttling and iEGR can help increase the
489 EGT while simultaneously minimising the levels of ISCO and ISHC [31]. Moreover, the low
490 combustion efficiency adversely affected the performance of the dual-fuel operation at 0.3 MPa
491 IMEP, limiting the net indicated efficiency to 38.9%.

492
493 Nonetheless, the ethanol-diesel dual-fuel combustion resulted in higher net indicated efficiencies
494 than the CDC operation between 0.6 and 2.4 MPa IMEP. A peak net indicated efficiency of 47.2%
495 was attained at 1.2 MPa IMEP and represented an increase of 4.4% over the 45.2% of the CDC
496 mode. The maximum net indicated efficiency achieved by the CDC operation was 45.7% at 1.5
497 MPa IMEP.

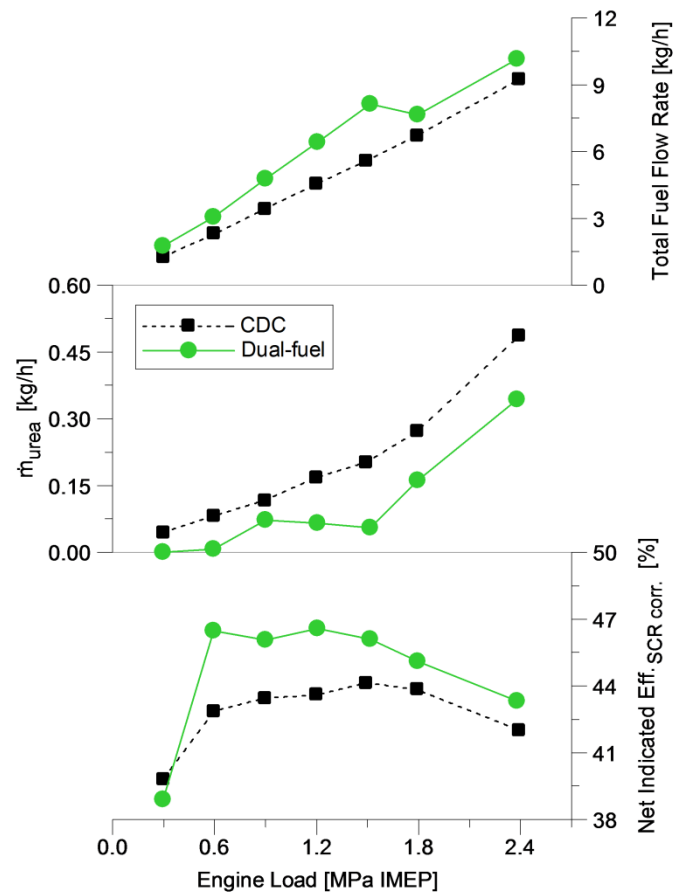
498 The ethanol autoignition process likely helped decrease the combustion temperatures and thus
499 the heat transfer losses [49], as supported by the NO_x reduction in Figure 8. However, the use of
500 a late CA50 at 1.5 MPa IMEP and low EFs at 1.8 and 2.4 MPa IMEP limited improvements in the
501 net indicated efficiency of the dual-fuel operation. This was necessary in order to control the PRRs
502 below 2.0 MPa/CAD.

504 4.6. Additional practical considerations

506 Additional practical aspects for ethanol-diesel dual-fuel operation were assessed in order to
507 evaluate whether the combustion strategy can be successfully used in a Euro VI HD engine. The
508 analysis focused on the total fuel flow rate, the estimated consumption of aqueous urea solution in
509 the SCR system (\dot{m}_{urea}) to meet the Euro VI NO_x limit of 0.4 g/kWh, and the SCR corrected net
510 indicated efficiency (*Net Indicated Eff_{SCR corr.}*). The methodology for the calculation of these
511 performance metrics has been described in our previous study [45].

513 Figure 10 shows the optimised ethanol-diesel dual-fuel combustion increased the total fuel
514 consumption by up to 45.8% in comparison with the CDC mode (8.12 kg/h vs. 5.57 kg/h at 1.5
515 MPa IMEP). This is attributed to the relatively lower density ($\rho_{ethanol}$) and energy content
516 ($LHV_{ethanol}$) of the ethanol fuel. Appropriate volumes of diesel and ethanol fuel tanks will have to
517 be designed according to the application of the engine and duty cycle.

519 In terms of NO_x aftertreatment, the ethanol-diesel dual-fuel combustion attained lower levels of
520 ISNO_x than the CDC operation, effectively decreasing the \dot{m}_{urea} requirements. Higher \dot{m}_{urea} were
521 estimated for both the combustion modes as the engine load was increased. This was due to an
522 increase in the production of NO_x emissions (in g/h) as well as the reduction in the EGR rate at
523 1.8 and 2.4 MPa IMEP.



525

526 Figure 10 – Practical considerations for optimised CDC and ethanol-diesel dual-fuel operation on a
 527 Euro VI HD engine.

528

529 The lower urea consumption in the dual-fuel mode allowed for higher *Net Indicated Eff.*_{SCR corr.}
 530 between 0.6 and 2.4 MPa IMEP. The maximum *Net Indicated Eff.*_{SCR corr.} of 46.5% was achieved
 531 at 0.6 MPa IMEP and represented an increase of 8.4% over the CDC mode. Impaired combustion
 532 efficiency limited the *Net Indicated Eff.*_{SCR corr.} of the dual-fuel mode at 0.3 MPa IMEP, despite
 533 the low engine-out NO_x of 0.4 g/kWh and $\dot{m}_{urea} = 0$.

534

535 These improvements can reduce the engine running costs depending on the volumetric price ratio
 536 between ethanol and diesel fuel [45] as well as the cost of aqueous urea solution. Nevertheless,
 537 the implementation of this dual-fuel combustion strategy on a HD engine would have to weigh the
 538 higher efficiency and lower NO_x emissions against the additional complexity and upfront cost of a
 539 port fuel injection system and extra fuel tank.

4.7. Potential CO₂ reduction

Table 4 reveals the complete combustion of ethanol can reduce the emissions of CO₂ by ~4% when compared to the combustion of diesel at a given energy input. However, practical ethanol energy fractions in dual-fuel mode vary between 0.00 and ~0.80 while the actual fuel energy consumption changes with the net indicated efficiency.

Table 4 – Hypothetical CO₂ emissions for diesel and ethanol combustion.

Property	Diesel	Ethanol
Normalised molecular composition	$CH_{1.825}O_{0.0014}$	$CH_3O_{0.5}$
Lower heating value (LHV_{fuel})	42.9 MJ/kg	26.9 MJ/kg [49]
Normalised molar mass (M_{fuel})	13.87 g/mol	23.03 g/mol
Mass of CO ₂ emissions per mole of fuel	44.01 gCO ₂ /mol	44.01 gCO ₂ /mol
Mass of CO ₂ emissions per mass of fuel	3.17 gCO ₂ /g	1.91 gCO ₂ /g
Mass of CO ₂ emissions per MJ of fuel	73.9 gCO ₂ /MJ	71 gCO ₂ /MJ
Specific CO ₂ emissions reduction	n/a	~4%

The use of the engine-out CO₂ emissions in the calculation of net indicated specific emissions of CO₂ (ISCO₂) would result in incorrect trends for a dual-fuel operation, with significant reductions at all engine loads. This is because of the partial oxidation of hydrocarbons and formation of CO. To remove the effect of incomplete combustion, the ISCO₂ (in g/kWh) was estimated using the Equation 3, which assumed a complete oxidation of the fuel injected to CO₂, either in-cylinder or in the aftertreatment system.

$$ISCO_2 = \left(\frac{\dot{m}_{diesel}}{M_{diesel}} + \frac{\dot{m}_{ethanol}}{M_{ethanol}} \right) \left(\frac{M_{CO_2}}{P_{ind}} \right) \times 10^3$$

(3)

where M_{CO_2} is the molar mass of CO₂ of 44.01 g/mol [50] and P_{ind} is the net indicated power in kW.

Figure 11 shows the optimised dual-fuel operation can achieve lower $ISCO_2$ than the CDC mode from 0.6 to 2.4 MPa IMEP. The potential CO_2 reduction introduced by the ethanol-diesel dual-fuel combustion varied between 1.8% and 7.5%. This improvement was a result of the increase in net indicated efficiency combined with higher hydrogen to carbon ratio of the ethanol fuel [59,60]. The low net indicated efficiency impaired the CO_2 reduction at 0.3 MPa IMEP, increasing the $ISCO_2$ by 3.7% when compared to the CDC mode.

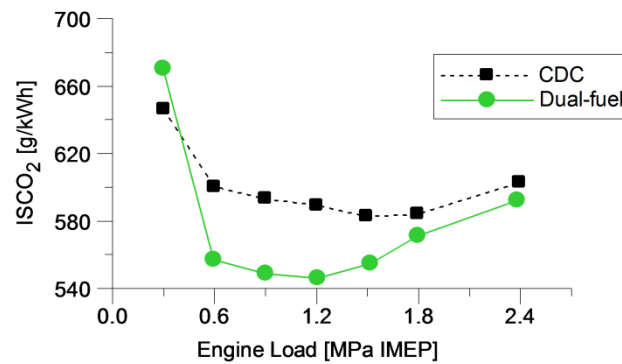


Figure 11 – Estimated $ISCO_2$ for optimised CDC and ethanol-diesel dual-fuel operation at 1200 rpm.

In order to provide an additional insight into the CO_2 reductions, a tank-to-wheels (TTW) analysis was performed by calculating the ratio of the estimated mass of CO_2 emissions to the total fuel energy supplied to the engine (in MJ) as

$$TTW CO_2 = \frac{ISCO_2 P_{ind}}{(\dot{m}_{diesel} LHV_{diesel} + \dot{m}_{ethanol} LHV_{ethanol})} \quad (4)$$

Figure 12 reveals the optimised ethanol-diesel dual-fuel combustion decreased the levels of TTW CO_2 emissions by up to 3.2% when compared against a constant 73.9 g/MJ produced by the CDC operation. This was attributed to the presence of the ethanol fuel, as the TTW CO_2 emissions are heavily dependent on the in-cylinder fuel characteristics (e.g. M_{fuel} and LHV_{fuel}).

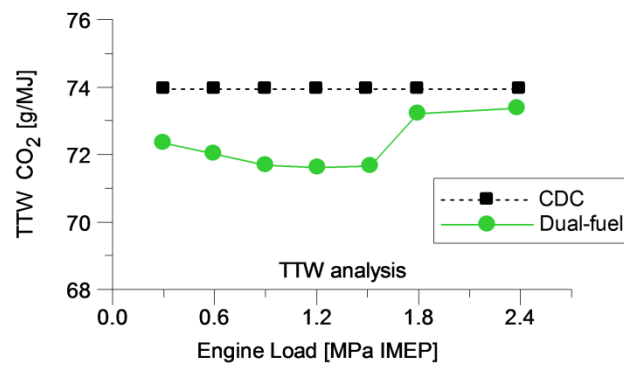


Figure 12 – Estimated TTW CO₂ emissions for CDC and ethanol-diesel dual-fuel operation.

It is important bear in mind that the data showed in Figure 11 and Figure 12 were obtained by assuming complete conversion of the fuel into ISCO₂. Additionally, the analysis neglected the CO₂ emissions produced by aqueous urea solution reactions in the SCR system [26], which were calculated [50] to be smaller than 0.4% of the estimated ISCO₂. For a more comprehensive analysis, the actual CO₂ emissions should be measured downstream of the aftertreatment system during the appropriate engine/vehicle test cycle.

4.8. Theoretical well-to-wheels analysis

A well-to-wheels (WTW) analysis can be used to assess the GHG emissions and energy expended over the production and use of a given fuel [37,44]. The methodology combines the TTW results to the well-to-tank (WTT) contribution, which takes into consideration the GHGs emitted during the extraction or cultivation of raw materials, processing, transportation, and other processes necessary to get the fuel into the fuel tank.

The levels of GHGs were expressed as grams of CO₂ equivalent (CO_{2eq}) emissions per MJ of fuel injected. This was required because of the higher global warming potentials (GWPs) for methane (CH₄) and nitrous oxide (N₂O) compounds, which have GWPs equivalent to 25 and 298 times that of the CO₂ over a time horizon of 100 years [61].

If one considers the CO₂ emissions from bioethanol combustion can be absorbed by plants during photosynthesis [37,44], the TTW CO_{2eq} emissions for a bioethanol-diesel dual-fuel engine will be determined by those emitted from diesel combustion only as

$$TTW CO_{2eq} = 73.9 (1 - EF) \quad (5)$$

From Equation 5, the WTW CO_{2eq} emissions were calculated as

$$WTW CO_{2eq} = [WTT_{diesel}(1 - EF) + WTT_{ethanol}(EF)] + TTW CO_{2eq} \quad (6)$$

where WTT_{diesel} is the WTT CO_{2eq} emissions for fossil diesel fuel of 15.4 g/MJ [38][39], and $WTT_{ethanol}$ is the WTT CO_{2eq} emissions for sugarcane ethanol of 24.8 g/MJ [38][39].

The $WTT_{ethanol}$ excluded CO_{2eq} emissions produced by indirect land use change (iLUC) due to the uncertainties over the predictions [62–64][65] and the possibility of a bonus if biomass is obtained from restored degraded land [36].

Figure 13 shows the theoretical TTW CO_{2eq} and WTW CO_{2eq} emissions for CDC and bioethanol-diesel dual-fuel operation. The lowest TTW CO_{2eq} emissions were attained at mid-loads under the dual-fuel mode, where both the net indicated efficiency and EF were maximised. As a result, the bioethanol-diesel dual-fuel combustion decreased the levels of WTW CO_{2eq} by up to 57% when compared with the 89.3 g/MJ for a CDC operation. These improvements can help combat climate change and achieve a more sustainable transport sector.

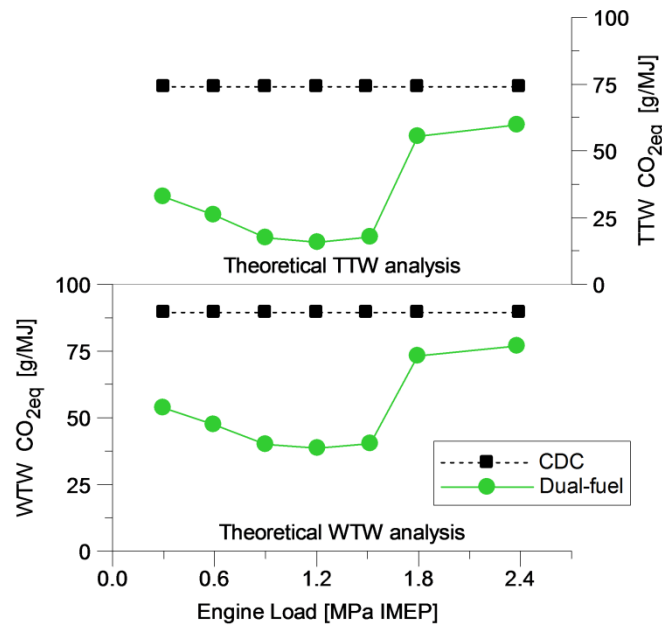


Figure 13 – Theoretical TTW and WTW CO_{2eq} emissions for CDC and bioethanol-diesel dual-fuel operation.

5. Conclusions

In this study, experiments were performed to compare the controllability, exhaust emissions, and fuel conversion efficiency of ethanol-diesel dual-fuel combustion to those of conventional diesel combustion (CDC). The investigation was conducted using identical operating conditions at a constant engine speed of 1200 rpm and different loads ranging between 0.3 and 2.4 MPa IMEP.

Testing was carried out on a HD diesel engine with a stock piston and original compression ratio of 16.8. Peak in-cylinder pressure and pressure rise rate (PRR) were limited at 18 MPa and 2.0 MPa/CAD, respectively. The diesel injection timings and fuel delivery were optimised for the maximum net indicated efficiency in both the combustion modes. The comparison against the CDC operation allowed for a better understanding of the potentials, requirements, and limitations of the ethanol-diesel dual-fuel combustion, which can be summarised as follows:

- 652 1. The dual-fuel combustion attained significantly lower NO_x and soot emissions than the
653 CDC cases at low engine loads of 0.3 and 0.6 MPa IMEP. This was attributed to the
654 combustion of more homogeneous charge obtained by the use of an early single diesel
655 injection at approximately -36 CAD ATDC and large percentages of premixed ethanol with
656 energy fractions of 0.56 and 0.65.
- 657 2. The dual-fuel mode experienced a relatively low net indicated efficiency of 38.9% at the
658 lowest load of 0.3 MPa IMEP. This was associated with the reduced combustion efficiency
659 of 88.7% caused by excessively lean and low temperature combustion. This region of
660 engine speed-load map also suffered from a low exhaust gas temperature of 463 K, which
661 can adversely affect the effectiveness of the oxidation catalyst.
- 662 3. Higher ethanol energy fractions up to 0.79 and adaptive diesel injections were required as
663 the engine load was increased from 0.6 to 1.5 MPa IMEP. A transition zone was observed
664 between 0.6 and 0.9 MPa IMEP where less diesel fuel could be partially premixed in order
665 to avoid early ignition and control the levels of PRR.
- 666 4. At mid-loads of 0.9, 1.2, and 1.5 MPa IMEP, optimised dual-fuel combustion was achieved
667 with a 3 mm³ diesel pre-injection prior to the main diesel injection. The relatively higher
668 degree of fuel stratification increased the levels of NO_x and soot when compared to those
669 obtained at low engine loads. Nevertheless, mid-load dual-fuel operation attained lower
670 NO_x emissions and up to 4.4% higher net indicated efficiencies than the CDC cases.
- 671 5. At high engine loads of 1.8 and 2.4 MPa IMEP, early autoignition of the ethanol fuel
672 increased the PRRs and limited the maximum ethanol energy fractions at 0.25 and 0.19,
673 respectively. This was linked to the high in-cylinder gas temperatures and pressures prior to
674 the start of combustion. Nonetheless, the ethanol compression ignition combustion helped
675 increase the net indicated efficiency and reduce NO_x emissions in comparison with the
676 CDC mode. This was primary due to a shorter diesel mixing-controlled combustion.

6. The ethanol-diesel dual-fuel combustion increased the total fuel flow rate by up to 45.8% when compared against the CDC operation. This was a result of differences in fuel characteristics (e.g. LHV_{fuel}) and will require the design of appropriate fuel tank volumes.

Overall, the optimisation of the diesel injection strategy and ethanol energy fraction was a key enabler for controlling the PRRs. This allowed for a dual-fuel combustion with higher net indicated efficiencies than the CDC operation between 0.6 and 2.4 MPa IMEP, with a peak of 47.2% at 1.2 MPa IMEP. Furthermore, the ethanol-diesel dual-fuel combustion attained lower NO_x emissions (up to 90%) than the CDC mode from low to full engine load. This can decrease the consumption of aqueous urea solution in the exhaust aftertreatment system and help to lower the engine running cost. Finally, the substitution of diesel with bioethanol (e.g. produced from sugarcane) can reduce the use of fossil fuel and effectively minimise the GHG emissions of future HD engines, as supported by the lower tank-to-wheels and theoretical well-to-wheels CO₂ equivalent emissions.

Acknowledgments

V. B. Pedrozo would like to acknowledge CAPES Foundation (Coordenação de Aperfeiçoamento de Pessoal de Nível Superior), research grant No. 13455/2013–03, for supporting his PhD study at Brunel University London under the supervision of Prof. Hua Zhao.

Nomenclature

ATDC, After Firing Top Dead Centre; CA10, Crank Angle of 10% Cumulative Heat Release; CA10–CA90, Combustion Duration or 10–90% Cumulative Heat Release; CA50, Crank Angle of 50% Cumulative Heat Release; CA90, Crank Angle of 90% Cumulative Heat Release; CAD, Crank Angle Degree; CDC, Conventional Diesel Combustion; CH₄, Methane; CO, Carbon Monoxide; CO₂, Carbon Dioxide; CO_{2eq}, CO₂ Equivalent; COV_{IMEP}, Coefficient of Variation of

704 IMEP; $COV_{P_{max}}$, Coefficient of Variation of P_{max} ; DAQ, Data Acquisition; ECU, Engine Control
 705 Unit; EF, Ethanol Energy Fraction; EGR, Exhaust Gas Recirculation; EGT, Exhaust Gas
 706 Temperature; FID, Flame Ionisation Detector; GHG, Greenhouse Gas; GWP, Global Warming
 707 Potential; HC, Hydrocarbons; HD; Heavy-duty; HRR, Apparent Net Heat Release Rate; iEGR,
 708 Internal EGR; iLUC, Indirect Land Use Change; IMEP, Net Indicated Mean Effective Pressure;
 709 ISCO, Net Indicated Specific Emissions of CO; $ISCO_2$, Net Indicated Specific Emissions of CO_2 ;
 710 ISHC, Net Indicated Specific Emissions of Actual Unburnt HC; ISNOx, Net Indicated Specific
 711 Emissions of NOx; ISsoot, Net Indicated Specific Emissions of Soot; LHV_{diesel} , Lower Heating
 712 Value of Diesel; $LHV_{ethanol}$, Lower Heating Value of Ethanol; LHV_{fuel} , Lower Heating Value; \dot{m}_{air} ,
 713 Fresh Air Mass Flow Rate; \dot{m}_{diesel} , Diesel Mass Flow Rate; $\dot{m}_{ethanol}$, Ethanol Mass Flow Rate;
 714 \dot{m}_{urea} , Estimated Consumption of Aqueous Urea Solution in the SCR System; M_{CO_2} , Normalised
 715 Molar Mass of CO_2 ; M_{diesel} , Normalised Molar Mass of Diesel; $M_{ethanol}$, Normalised Molar Mass of
 716 Ethanol; M_{fuel} , Normalised Molar Mass; MFB, Mass Fraction Burnt; N_2O , Nitrous Oxide;
 717 $Net\ Indicated\ Eff_{SCR\ corr.}$, SCR Corrected Net Indicated Efficiency; NOx, Nitrogen Oxides; O_2 ,
 718 Oxygen; P_{ind} , Net Indicated Power; PFI, Port Fuel Injector; P_{max} , Peak In-cylinder Gas Pressure;
 719 PRR, Pressure Rise Rate; RON, Research Octane Number; SCR, Selective Catalyst Reduction;
 720 SOC, Start of Combustion; SOI_{main}, Actual Start of Main Diesel Injection; SOI_{mai}–SOC,
 721 Ignition Delay; SOI_{pre}, Actual Start of Diesel Pre-injection; TDC, Firing Top Dead Centre; TTW,
 722 Tank-to-wheels; VVA, Variable Valve Actuation; WTT, Well-to-tank; WTT_{diesel} , WTT CO_{2eq}
 723 Emissions for Fossil Diesel; $WTT_{ethanol}$, WTT CO_{2eq} Emissions for Ethanol; WTW, Well-to-wheels;
 724 $\%C_{fuel}$, Carbon Mass Content; $\%H_{fuel}$, Hydrogen Mass Content; $\%O_{fuel}$, Carbon Mass Content; γ ,
 725 Ratio of Specific Heats; ρ_{fuel} , Density; ρ_{diesel} , Diesel Density; $\rho_{ethanol}$, Ethanol Density; Φ , Global
 726 Fuel/Air Equivalence Ratio.

727

728 References

- 729 [1] Intergovernmental Panel on Climate Change (IPCC). Climate Change 2014 - Synthesis
730 Report. IPCC Fifth Assessment Report 2015:1–112.
- 731 [2] United States Environmental Protection Agency. Climate Change Indicators: Atmospheric
732 Concentrations of Greenhouse Gases. EPA's Climate Change Indicators 2016.
733 [https://www.epa.gov/climate-indicators/climate-change-indicators-atmospheric-](https://www.epa.gov/climate-indicators/climate-change-indicators-atmospheric-concentrations-greenhouse-gases)
734 [concentrations-greenhouse-gases](https://www.epa.gov/climate-indicators/climate-change-indicators-atmospheric-concentrations-greenhouse-gases) (accessed July 4, 2017).
- 735 [3] Miller JD, Façanha C. The state of clean transport policy - A 2014 synthesis of vehicle and
736 fuel policy developments. The ICCT Report 2014:73.
- 737 [4] Kodjak D. Policies to reduce fuel consumption, air pollution, and carbon emissions from
738 vehicles in G20 nations. The ICCT Briefing Paper 2015:28.
- 739 [5] Dec JE. A conceptual model of DI diesel combustion based on laser sheet imaging. SAE
740 Technical Paper 1997. doi:10.4271/970873.
- 741 [6] Kokjohn SL, Hanson RM, Splitter D a, Reitz RD. Fuel reactivity controlled compression
742 ignition (RCCI): a pathway to controlled high-efficiency clean combustion. International
743 Journal of Engine Research 2011;12:209–26. doi:10.1177/1468087411401548.
- 744 [7] Musculus MPB, Miles PC, Pickett LM. Conceptual models for partially premixed low-
745 temperature diesel combustion. Progress in Energy and Combustion Science 2013;39.
746 doi:10.1016/j.pecs.2012.09.001.
- 747 [8] Reitz RD. Directions in internal combustion engine research. Combustion and Flame
748 2013;160:1–8. doi:10.1016/j.combustflame.2012.11.002.

- 749 [9] Iwabuchi Y, Kawai K, Shoji T, Takeda Y. Trial of New Concept Diesel Combustion System -
750 Premixed Compression-Ignited Combustion -. SAE Technical Paper 1999.
751 doi:10.4271/1999-01-0185.
- 752 [10] World Health Organization. WHO Air quality guidelines for particulate matter, ozone,
753 nitrogen dioxide and sulfur dioxide. 2006.
- 754 [11] World Health Organization. Global health risks - Mortality and burden of disease attributable
755 to selected major risks. Geneva: 2009.
- 756 [12] Environmental Protection Agency (EPA) - National Highway Traffic Safety Administration
757 (NHTSA) - Department of Transportation (DOT). Greenhouse Gas Emissions and Fuel
758 Efficiency Standards for Medium- and Heavy-Duty Engines and Vehicles. Federal Register -
759 Rules and Regulations 2011;76.
- 760 [13] Environmental Protection Agency (EPA) - National Highway Traffic Safety Administration
761 (NHTSA) - Department of Transportation (DOT). Greenhouse Gas Emissions and Fuel
762 Efficiency Standards for Medium- and Heavy-Duty Engines and Vehicles - Phase 2. Federal
763 Register - Rules and Regulations 2016;81.
- 764 [14] The European Parliament and the Council of the European Union. Regulation (EC) No
765 595/2009. Official Journal of the European Union 2009;188.
- 766 [15] The European Parliament and the Council of the European Union. Commission Regulation
767 (EU) No 582/2011. Official Journal of the European Union 2011;167.
- 768 [16] Posada F, Chambliss S, Blumberg K. Costs of emission reduction technologies for heavy-
769 duty diesel vehicles. The ICCT White Paper 2016.

- 770 [17] Delgado O, Rodríguez F, Muncrief R. Fuel Efficiency Technology in European Heavy-Duty
771 Vehicles: Baseline and Potential for the 2020-2030 Time Frame. The ICCT White Paper
772 2017.
- 773 [18] Görsmann C. Improving air quality while reducing the emission of greenhouse gases.
774 Johnson Matthey Technology Review 2015;59:139–51. doi:10.1595/205651315X687524.
- 775 [19] O'Connor J, Borz M, Ruth D, Han J, Paul C, Imren A, et al. Optimization of an Advanced
776 Combustion Strategy Towards 55% BTE for the Volvo SuperTruck Program. SAE
777 International Journal of Engines 2017;10:2017–01 – 0723. doi:10.4271/2017-01-0723.
- 778 [20] Stanton D, Charlton S, Vajapeyazula P. Diesel Engine Technologies Enabling Powertrain
779 Optimization to Meet U.S. Greenhouse Gas Emissions. SAE International Journal of
780 Engines 2013;6. doi:10.4271/2013-24-0094.
- 781 [21] López - De Jesús YM, Chigada PI, Watling TC, Arulraj K, Thorén A, Greenham N, et al. NOx
782 and PM Reduction from Diesel Exhaust Using Vanadia SCR[®]. SAE International Journal
783 of Engines 2016;9:2016–01 – 0914. doi:10.4271/2016-01-0914.
- 784 [22] Walker A, Johnson Matthey. Catalyst-Based Emission Control Solutions for the Global HDD
785 Market – What Does the Future Hold? Presentation at SAE 2016 Heavy-Duty Diesel
786 Emissions Control Symposium, Gothenburg: 2016.
- 787 [23] Delgado O, Lutsey N. The U.S. SuperTruck Program: Expediting the development of
788 advanced heavy-duty vehicle efficiency technologies. The ICCT White Paper 2014.
- 789 [24] Charlton S, Dollmeyer T, Grana T. Meeting the US Heavy-Duty EPA 2010 Standards and
790 Providing Increased Value for the Customer. SAE International Journal of Commercial
791 Vehicles 2010;3. doi:10.4271/2010-01-1934.

- 792 [25] Johnson T V. Diesel Emissions in Review. SAE International Journal of Engines 2011;4.
793 doi:10.4271/2011-01-0304.
- 794 [26] Stanton DW. Systematic Development of Highly Efficient and Clean Engines to Meet Future
795 Commercial Vehicle Greenhouse Gas Regulations. SAE International Journal of Engines
796 2013;6. doi:10.4271/2013-01-2421.
- 797 [27] Liu J, Wang H, Zheng Z, Zou Z, Yao M. Effects of Different Turbocharging Systems on
798 Performance in a HD Diesel Engine with Different Emission Control Technical Routes. SAE
799 Technical Paper 2016. doi:10.4271/2016-01-2185.
- 800 [28] Dallmann T, Menon A. Technology Pathways for Diesel Engines Used in Non-Road
801 Vehicles and Equipment. The ICCT White Paper 2016.
- 802 [29] Pedrozo VB, May I, Dalla Nora M, Cairns A, Zhao H. Experimental analysis of ethanol dual-
803 fuel combustion in a heavy-duty diesel engine: An optimisation at low load. Applied Energy
804 2016;165:166–82. doi:10.1016/j.apenergy.2015.12.052.
- 805 [30] Pedrozo VB, May I, Zhao H. Characterization of Low Load Ethanol Dual-Fuel Combustion
806 using Single and Split Diesel Injections on a Heavy-Duty Engine. SAE Technical Paper
807 2016. doi:10.4271/2016-01-0778.
- 808 [31] Pedrozo VB, May I, Lanzasova TDM, Zhao H. Potential of internal EGR and throttled
809 operation for low load extension of ethanol–diesel dual-fuel reactivity controlled compression
810 ignition combustion on a heavy-duty engine. Fuel 2016;179:391–405.
811 doi:10.1016/j.fuel.2016.03.090.
- 812 [32] Tong D, Ren S, Li Y, Wang Z, Zhang H, Wang Z, et al. Performance and emissions of
813 gasoline Homogeneous Charge Induced Ignition (HCII) by diesel through whole operating
814 range on a heavy-duty multi-cylinder engine. Fuel 2017;197:259–71.
815 doi:10.1016/j.fuel.2017.02.003.

- 816 [33] Divekar P, Han X, Tan Q, Asad U, Yanai T, Chen X, et al. Mode Switching to Improve Low
817 Load Efficiency of an Ethanol-Diesel Dual-Fuel Engine. SAE Technical Paper 2017.
818 doi:10.4271/2017-01-0771.
- 819 [34] May I, Pedrozo V, Zhao H, Cairns A, Whelan S, Wong H, et al. Characterization and
820 Potential of Premixed Dual-Fuel Combustion in a Heavy Duty Natural Gas/Diesel Engine.
821 SAE Technical Paper 2016. doi:10.4271/2016-01-0790.
- 822 [35] Li J, Yang W, Zhou D. Review on the management of RCCI engines. *Renewable and*
823 *Sustainable Energy Reviews* 2017;69:65–79. doi:10.1016/j.rser.2016.11.159.
- 824 [36] The European Parliament and the Council of the European Union. Directive 2009/28/EC.
825 Official Journal of the European Union 2009;140.
- 826 [37] Edwards R, Larivé J-F, Rickeard D, Weindorf W. Well-to-Wheels analysis of future
827 automotive fuels and powertrains in the European context: Well-to-Tank Report - Version
828 4.a. Joint Research Centre of the European Commission, EUCAR, and CONCAWE
829 2014;4.a. doi:10.2790/95629.
- 830 [38] Edwards R, Larivé J-F, Rickeard D, Weindorf W. Well-to-Wheels analysis of future
831 automotive fuels and powertrains in the European context: Well-to-Tank Appendix 2 -
832 Version 4a. Joint Research Centre of the European Commission, EUCAR, and CONCAWE
833 2014:1–133. doi:10.2790/95629.
- 834 [39] Edwards R, Hass H, Larivé J-F, Rickeard D, Weindorf W. Well-to-Wheels analysis of future
835 automotive fuels and powertrains in the European context: Well-to-Tank Appendix 4 -
836 Version 4a. Joint Research Centre of the European Commission, EUCAR, and CONCAWE
837 2014. doi:10.2790/95629.

- 838 [40] Jaiswal D, De Souza AP, Larsen S, LeBauer DS, Miguez FE, Sparovek G, et al. Brazilian
839 sugarcane ethanol as an expandable green alternative to crude oil use. *Nature Climate*
840 *Change* 2017;7:788–92. doi:10.1038/nclimate3410.
- 841 [41] Molina S, García a., Pastor JM, Belarte E, Balloul I. Operating range extension of RCCI
842 combustion concept from low to full load in a heavy-duty engine. *Applied Energy*
843 2015;143:211–27. doi:10.1016/j.apenergy.2015.01.035.
- 844 [42] Benajes J, García A, Monsalve-Serrano J, Boronat V. Achieving clean and efficient engine
845 operation up to full load by combining optimized RCCI and dual-fuel diesel-gasoline
846 combustion strategies. *Energy Conversion and Management* 2017;136:142–51.
847 doi:10.1016/j.enconman.2017.01.010.
- 848 [43] Benajes J, García A, Monsalve-Serrano J, Boronat V. Gaseous emissions and particle size
849 distribution of dual-mode dual-fuel diesel-gasoline concept from low to full load. *Applied*
850 *Thermal Engineering* 2017;120:138–49. doi:10.1016/j.applthermaleng.2017.04.005.
- 851 [44] Ramachandran S, Stimming U. Well to wheel analysis of low carbon alternatives for road
852 traffic. *Energy Environ Sci* 2015;8:3313–24. doi:10.1039/C5EE01512J.
- 853 [45] Pedrozo VB, May I, Zhao H. Exploring the mid-load potential of ethanol-diesel dual-fuel
854 combustion with and without EGR. *Applied Energy* 2017;193:263–75.
855 doi:10.1016/j.apenergy.2017.02.043.
- 856 [46] Pedrozo VB, Zhao H. Improvement in high load ethanol-diesel dual-fuel combustion by
857 Miller cycle and charge air cooling. *Applied Energy* 2018;210:138–51.
858 doi:10.1016/j.apenergy.2017.10.092.
- 859 [47] Schwoerer J, Kumar K, Ruggiero B, Swanbon B. Lost-Motion VVA Systems for Enabling
860 Next Generation Diesel Engine Efficiency and After-Treatment Optimization. *SAE Technical*
861 *Paper* 2010. doi:10.4271/2010-01-1189.

- 862 [48] International Organisation of Legal Metrology (IOLM). International Recommendation No22 -
863 Alcoholometry. First Ed. Paris: 1973.
- 864 [49] Heywood JB. Internal Combustion Engine Fundamentals. First Ed. McGraw-Hill, Inc.; 1988.
- 865 [50] Economic Commission for Europe of the United Nations (UN/ECE). Regulation No 49 -
866 Uniform provisions concerning the measures to be taken against the emission of gaseous
867 and particulate pollutants from compression-ignition engines and positive ignition engines for
868 use in vehicles. Official Journal of the European Union 2013;171.
- 869 [51] Kar K, Cheng WK. Speciated Engine-Out Organic Gas Emissions from a PFI-SI Engine
870 Operating on Ethanol/Gasoline Mixtures. SAE International Journal of Fuels and Lubricants
871 2009;2. doi:10.4271/2009-01-2673.
- 872 [52] Wallner T. Correlation Between Speciated Hydrocarbon Emissions and Flame Ionization
873 Detector Response for Gasoline/Alcohol Blends. Journal of Engineering for Gas Turbines
874 and Power 2011;133. doi:10.1115/1.4002893.
- 875 [53] May IA. An experimental investigation of lean-burn dual-fuel combustion in a heavy duty
876 diesel engine. Brunel University London, 2017.
- 877 [54] Zhao H. Advanced direct injection combustion engine technologies and development -
878 Volume 2: Diesel engines. Cambridge: Woodhead Publishing Limited; 2010.
- 879 [55] Park C, Busch S. The influence of pilot injection on high-temperature ignition processes and
880 early flame structure in a high-speed direct injection diesel engine. International Journal of
881 Engine Research 2017. doi:10.1177/1468087417728630.
- 882 [56] Desantes JM, Benajes J, García A, Monsalve-Serrano J. The role of the in-cylinder gas
883 temperature and oxygen concentration over low load reactivity controlled compression
884 ignition combustion efficiency. Energy 2014;78:854–68. doi:10.1016/j.energy.2014.10.080.

- 885 [57] Tsang KS, Zhang ZH, Cheung CS, Chan TL. Reducing Emissions of a Diesel Engine Using
886 Fumigation Ethanol and a Diesel Oxidation Catalyst. *Energy & Fuels* 2010;24.
887 doi:10.1021/ef100899z.
- 888 [58] Prikhodko VY, Curran SJ, Parks JE, Wagner RM. Effectiveness of Diesel Oxidation Catalyst
889 in Reducing HC and CO Emissions from Reactivity Controlled Compression Ignition. *SAE*
890 *International Journal of Fuels and Lubricants* 2013;6. doi:10.4271/2013-01-0515.
- 891 [59] Di Blasio G, Beatrice C, Molina S. Effect of Port Injected Ethanol on Combustion
892 Characteristics in a Dual-Fuel Light Duty Diesel Engine. *SAE Technical Paper* 2013;01.
893 doi:10.4271/2013-01-1692.
- 894 [60] Han X, Yang Z, Wang M, Tjong J, Zheng M. Clean combustion of n-butanol as a next
895 generation biofuel for diesel engines. *Applied Energy* 2016.
896 doi:10.1016/j.apenergy.2016.12.059.
- 897 [61] Intergovernmental Panel on Climate Change (IPCC). *Climate Change 2007: The Physical*
898 *Science Basis. Contribution of Working Group I to the Fourth Assessment Report of the*
899 *Intergovernmental Panel on Climate Change 2007.*
- 900 [62] Laborde D. *Assessing the Land Use Change Consequences of European Biofuel Policies.*
901 *International Food Policy Institute (IFPRI), 2011.*
- 902 [63] Wang M, Han J, Dunn JB, Cai H, Elgowainy A. Well-to-wheels energy use and greenhouse
903 gas emissions of ethanol from corn, sugarcane and cellulosic biomass for US use.
904 *Environmental Research Letters* 2012;7:045905. doi:10.1088/1748-9326/7/4/045905.
- 905 [64] Yan X, Boies AM. Quantifying the uncertainties in life cycle greenhouse gas emissions for
906 UK wheat ethanol. *Environmental Research Letters* 2013;8:015024. doi:10.1088/1748-
907 9326/8/1/015024.

- 908 [65] Morganti K, Al-Abdullah M, Alzubail A, Kalghatgi G, Viollet Y, Head R, et al. Synergistic
909 engine-fuel technologies for light-duty vehicles: Fuel economy and Greenhouse Gas
910 Emissions. *Applied Energy* 2017;208:1538–61. doi:10.1016/j.apenergy.2017.08.213.

911